Atmospheric and Ionospheric Electromagnetic Phenomena Associated with Earthquakes,
Ed. M. Hayakawa, pp. 287–305.

A Model for the Generation of Precursory Electric and Magnetic Fields Associated with the Deformation Rate of the Earthquake Focus

Filippos VALLIANATOS[1] and Andreas TZANIS[2]

[1]*Technological Educational Institute of Crete, Chania Branch, 3 Romanou Str., Chalepa, 73133 Chania, Crete, Greece*
[2]*Department of Geophysics-Geothermy, University of Athens, Athens, Panepistimiopoli, GR-15784, Greece*

Abstract. We present a model for the generation of electric current in rocks under stress, involving the strain rate, ($\dot{\varepsilon}$) which is influenced by the motion of charge bearing dislocations. The relationship between current density and strain rate is demonstrated. On the basis of laboratory data, we estimate the deformation rate necessary to generate an electric signal observable at distances far enough from the source, as to qualify it as an electric earthquake precursor. Using this mechanism and the geometrical characteristics of such a type of source we simulate the propagation of the electric and magnetic fields and their "received" characteristics as a function of the source-receiver separation. We find that the magnetic field is an effective indicator of the quality of the source, in particular due to its spatial properties (azimuthal variation) and the relationship between the horizontal and vertical components. We conclude that the expected signal waveforms at long distances from such a kind of source are similar to a class of signals (bay like waveforms), independently observed prior to earthquakes by several investigators.

1. Introduction

The generation of electric currents in rocks under stress has long been recognized by means of experiment. For instance, Whitworth[1)] has demonstrated such an effect in alkali halides under pressure. In a more recent paper[2)], the generation of electric current in rocks under uniaxial compression is reported. The main result of these investigations is that the shape of the electric signal depends drastically on the rate of stress variation and specifically, appears to follow the first derivative of the externally applied stress. From a theoretical point of view, two types of current generation mechanisms have been studied. The first is reported by Varotsos *et al.*[3)], and is related to polarization or depolarization effects. The second by Slifkin[4)], is based on the concept of motion of charged dislocations. In the present paper, we discuss the available data on the basis of the

moving charged dislocations (MCD) model. Furthermore, and assuming that the earthquake focus may be described by such a model, we make a first attempt to simulate the propagation of the resulting transient electric signal and describe its received characteristics at intermediate-long distances from the source (the earthquake in preparation).

2. A Current Generation Mechanism in Rocks under Pressure

In a crystalline structure, dislocations may be formed by an excess or absence of a half-plane of atoms. The edge of this half-plane comprises a dislocation line, around which the physical fields related with it are concentrated. In an ionic structure there will be an excess or absence of a line row of ions along the dislocation line, with consequence that the dislocation becomes charged. We note that the jogs of edge dislocation can be ionically charged. Whitworth[1] writes that a dislocation line "*in a thermal equilibrium would be surrounded by a cloud of point defects of the opposite sign to maintain electric neutrality and its dislocation core presence would therefore affect the concentration of point defects in the crystal*". However, in dynamic processes, when dislocations move, the electric neutrality can no longer be maintained.

Let Λ^+ be the density of edge dislocations of the type required to accommodate the uniaxial compression (or tension) and Λ^- be the density of dislocation of the opposite type. The motion of charged dislocations produces a transverse polarization:

$$P = \left(\Lambda^+ - \Lambda^-\right) \cdot q_l \cdot \frac{\delta x}{\sqrt{2}} = \delta\Lambda \cdot q_l \cdot \frac{\delta x}{\sqrt{2}} \tag{1}$$

where q_l is the charge per unit length on the dislocation. If screw dislocations are ignored, the plastic contribution to the strain, when these dislocations of Burger vector $\boldsymbol{b}$ move through a distance δx, is

$$\varepsilon_P = \left(\Lambda^+ + \Lambda^-\right) \cdot \boldsymbol{b} \cdot \frac{\delta x}{2}. \tag{2}$$

The rate of change in polarization is equivalent to the electric current density, by definition

$$J_P = \frac{\partial P}{\partial t} \xrightarrow{(1),(2)} J_P = \frac{\sqrt{2}}{\beta} \cdot \frac{q_l}{\boldsymbol{b}} \cdot \dot{\varepsilon}_P, \quad \beta = \frac{\Lambda^+ + \Lambda^-}{\Lambda^+ - \Lambda^-} \tag{3}$$

where β is a constant usually between 1 and 1.5. Equation (3) shows that the observed transient electric variation is related to the non-stationary accumulation of deformation. Specifically, when the deformation rate increases at a variable

Table 1. Stress sensitivity coefficient for various rocks estimated using data from Hadjicontis and Mavromatou.[2)]

Type of rock	E/(dσ/dt) [(V/m)/(bar/s)]
Ioannina limestone	0.70
Granite (sample A)	0.46
Granite (sample B)	0.32
mineral quartz	1.14

rate (i.e., $\dot{\varepsilon} > 0$ and $\ddot{\varepsilon} \neq 0$), then two cases are recognized:

1. If $\ddot{\varepsilon} > 0$ ($\ddot{\varepsilon} < 0$) then $\dot{E} > 0$ ($\dot{E} < 0$), meaning that an increase (decrease) of the observed electric field variation will result.

2. If $\dot{\varepsilon} > 0$ and $\ddot{\varepsilon} = 0$ (i.e., $\dot{\varepsilon}$ is constant with time) then E is also a constant. For a number of alkali and silver halides, experimental values have been deduced for the charge density[1)]. A typical value is of the order of $0.1e/\alpha$ where e is the electronic charge and α the lattice spacing[1)]. If we assume comparable figures for the rocks and take α to be about 5×10^{-10} m then the charge per unit length is of the order of 3×10^{-11} Cb/m (e.g. see Slifkin[4)]). Assuming that $\dot{\sigma} \approx Y\dot{\varepsilon}$, ($Y$ the Young modulus), the stress sensitivity coefficient F originally introduced by Vallianatos[5)] and Nomicos and Vallianatos[6)], is:

$$F = \frac{E}{(d\sigma)/(dt)} \approx \frac{\sqrt{2}}{\beta} \cdot \frac{q_l}{b} \cdot \frac{\rho}{Y} \tag{4}$$

where E is the observed electric field and ρ is the specific resistivity of the material. For the sake of comparison, we now proceed to estimate the order of magnitude of F.

Introducing in Eq. (4) above the values $b \approx 5 \times 10^{-10}$ m, $\rho \approx 10^7$ Ωm, and $Y \approx 0.8$ Mbar, we find $E/(d\sigma/dt) \approx 0.75$ (V/m)/(bar/s), which is comparable to the values calculated using the experimental data (see Table 1).

3. The Resulting Electric Signal—Geophysical Implications

We shall, now, attempt to present an analysis of the observed preseismic variations based on the MCD model[4),6)]. According to this model all rocks contain crystalline materials which already bear linear defects (i.e., charged edge dislocations), either inherently, or/and due to previous loading (deformation) cycles. Now consider that an earthquake zone comprises a volume filled by cracks or, equivalently, dislocation arrays[7)] (i.e. a concentration of charged dislocations). Thus, the processes of earthquake preparation (i.e., the non-linear evolution of stress) and energy release are determined by the evolution, propagation and nucleation of these defects and changes in their density.

This model of the earthquake source allows for the generation of electric current, with intensity proportional to the velocity of propagation of the MCD and to their density. The current density vector at the source is parallel to the velocity vector. Then, the horizontal component of the electric field, measured at a point on the surface with an epicentral distance x m from the source and at time t_K, may be qualitatively expressed as[5),8)]:

$$E(x,t_K) \approx sf_1\rho\sum(\rho_{dii}\cdot\upsilon_{mi})\frac{x-x_i(t_K)}{R_i^n(t_K)} \tag{5a}$$

where R_i is the distance of the observation point from the MCD element located at x_i, $n=2$ for a linear source, ρ_{di} is the CD density at point x_i, υ_{mi} is the dislocation velocity at x_i, s is a sensitivity coefficient at the location of the receiver and f_1 is a coefficient dependent on the geometry of the source. We emphasize that expression (5a) is based on the assumption that the time sequence of stress evolution is the same at each point on the source plane, only shifted by the time delay required for crack propagation. The macroscopic deformation rate, $\dot{\varepsilon}_i$ is related to the MCD density and velocity via a generalization of the Orowan's law ($\dot{\varepsilon} \approx \rho_{di}\cdot\upsilon_i$), and therefore (5a) becomes[6)]:

$$E(x,t_K) \approx sf_2\rho\sum\dot{\varepsilon}_i\frac{x-x_i(t_K)}{R_i^n(t_K)} \tag{5b}$$

where f_2 is also a factor dependent on the source. According to many models[9)], the development of processes prior to an earthquake may be qualitatively described in terms of four stages (I–IV) as shown in Fig. 1. Consider a volume within a statistically homogeneous medium, subject to stress increasing with time. During Stage I there exists a gradual increase in crack density with time; this Stage does appear to associate with electric preseismic phenomena. When the crack density exceeds a certain critical level, the natural interaction of cracks accelerates their development, causing an avalanche during Stage II. As a result, we observe a rapid increase in strain rate and the appearance of an anomalous electric field variation (see Fig. 1). In the last Stage IV of the process (i.e. in the failure stage) a "co-seismic" electric pulse may appear. In a series of models, Stuart[10)] indicated that strain accumulation should become non-linear near the end of the loading cycle. Thus considerably accelerated deformation effects should be produced during the last several days (1–10) prior to the earthquake; this defines the duration of Stage II and is consistent with the observed time lag between the anomalous electric field variation and the ensuing earthquake[6)].

Let us, now, consider the deformation rate necessary to generate the level of the observed preseismic transient electric variations, which are of the order of 2×10^{-5} V/m. Using the stress sensitivity $E/(d\sigma/dt)$ for the granite of Table 1, a

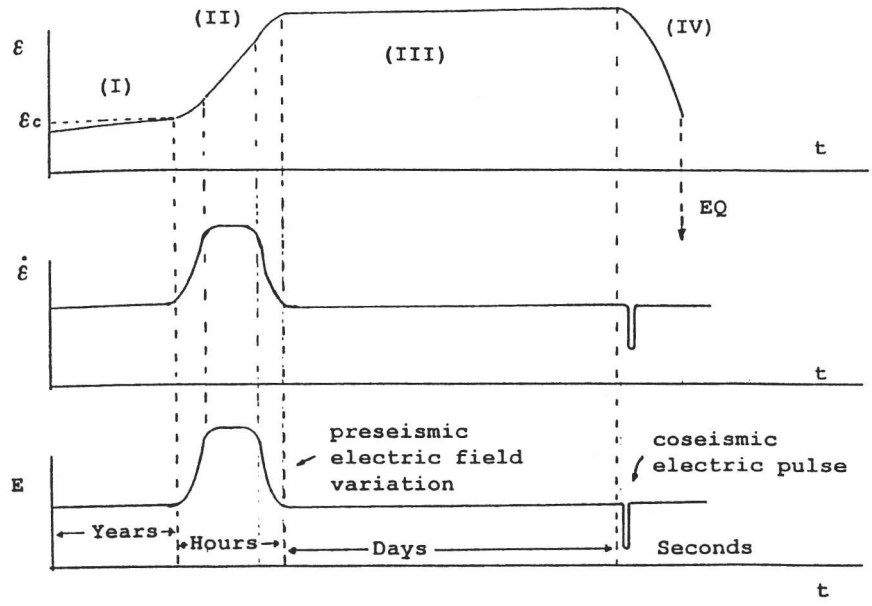

Fig. 1. Diagram, in arbitrary time scale, depicting the deformation (top), the deformation rate (middle) and the corresponding electric field variation (bottom) during the preparatory stage of an earthquake.

stress rate of 6.6×10^{-5} bar/s would be required, assuming that the signal does not decay over the distance of 100–300 km between measurement the receiver and the hypocenter. Stress is very difficult to measure geologically, but strain is more commonly measured. In order to convert this stress rate to a strain rate, we assume a homogeneous, linear, isotropic medium, composed of granite with a Young's modulus of 0.66 Mbar. Then the calculated stress rate becomes a strain rate of $10^{-10}\,s^{-1}$. A similar calculation for a sample of limestone from the area of Ioannina (Greece), with Young modulus 0.94 Mbar, leads to a strain rate of $3 \times 10^{-11}\,s^{-1}$. We note that these estimated strain rates are respectively 3333 and 1000 times higher than a typical geological strain rate of $3 \times 10^{-14}\,s^{-1}$ (i.e. 10 cm/yr) on a 100 km long fault. They are also 50 (for granite) and 15 (for limestone) times larger than the precursory change which was anticipated for the (expected but not realized) M6 Parkfield earthquake, and therefore, appear to be higher than what might be geologically expected. However, such strain rates are not impossible to achieve (S. Park, private communication). For instance, Wakita[11] provides an illustration of precursory strain changes for the M7 Izu-Oshima-kinkai earthquake of 14 January 1978. A careful study of this figure indicates that the strain rate could easily have reached the value of 10^{-11}–$10^{-12}\,s^{-1}$. Note also that an absolute lower threshold for the excitation of the crust by MCD should be the strain rate at the elastic tidal level ($\sim 4 \times 10^{-13}\,s^{-1}$ if $\varepsilon_{tidal} = 10^{-7}$).

4. Propagation of the Electric and Magnetic Signal

The MCD current generation mechanism described in the foregoing, amounts to the superposition of a large number of dipole sources, each dipole being an individual propagating crack or a cluster of simultaneously moving dislocations. In the following, we will attempt to investigate the behavior of this type of source at distances of several tens to a few hundreds of km. In doing so,

1. We assume that the source is a 3-D volume (cell) within the earthquake preparation zone filled with cracks which are excited coherently. Coherence is not a physical requirement; it is, however, a convenient first approximation and simplifies the computations.
2. By superimposing individual dipole fields in a coherent cell, we estimate upper limits for the expected amplitudes of the received transient fields.
3. We attempt to gain insight into the received characteristics (waveforms) of the transient fields by simulating the propagation of a pulse from an individual dipole and an individual cell. In order to demonstrate our arguments, herein we only consider propagation in a uniform half space.

The electromagnetic field at a point z in a conducting half space, due to a horizontal electric dipole buried at a depth d, can be expressed in terms of a sum of the direct field, the ideal reflected field or field of an ideal image and the rest of the field (King *et al.*[12]). This last part includes a lateral-wave field and correction terms for the reflected field to account for the fact that it may be not, actually, that of an ideal image. For instance, the radial electric field is:

$$E_R(\omega, R, \varphi, z) = -\frac{\omega\mu_0}{4\pi k^2}\cos\varphi\left[F_{R0}(R, z-d) + F_{R0}(R, z+d) + F_{R1}(R, z+d)\right]$$

where

$$F_{R0}(R, z-d) = \int_0^\infty \left(\frac{\gamma_1}{2}\left[J_0(\lambda R) - J_2(\lambda R)\right] + \frac{k_1^2}{2\gamma_1}\left[J_0(\lambda R) - J_2(\lambda R)\right]\right) e^{i\gamma_1|z-d|}\lambda d\lambda,$$

$$F_{R0}(R, z+d) = \int_0^\infty \left(\frac{\gamma_1}{2}\left[J_0(\lambda R) - J_2(\lambda R)\right] + \frac{k_1^2}{2\gamma_1}\left[J_0(\lambda R) - J_2(\lambda R)\right]\right) e^{i\gamma_1|z+d|}\lambda d\lambda,$$

$$F_{R1}(R, z+d)$$
$$= \int_0^\infty \left(\frac{\gamma_1}{2}(Q-1)\left[J_0(\lambda R) - J_2(\lambda R)\right] + \frac{k_1^2}{2\gamma_1}(P+1)\left[J_0(\lambda R) - J_2(\lambda R)\right]\right) e^{i\gamma_1|z-d|}\lambda d\lambda,$$

4. Propagation of the Electric and Magnetic Signal

The MCD current generation mechanism described in the foregoing, amounts to the superposition of a large number of dipole sources, each dipole being an individual propagating crack or a cluster of simultaneously moving dislocations. In the following, we will attempt to investigate the behavior of this type of source at distances of several tens to a few hundreds of km. In doing so,

1. We assume that the source is a 3-D volume (cell) within the earthquake preparation zone filled with cracks which are excited coherently. Coherence is not a physical requirement; it is, however, a convenient first approximation and simplifies the computations.
2. By superimposing individual dipole fields in a coherent cell, we estimate upper limits for the expected amplitudes of the received transient fields.
3. We attempt to gain insight into the received characteristics (waveforms) of the transient fields by simulating the propagation of a pulse from an individual dipole and an individual cell. In order to demonstrate our arguments, herein we only consider propagation in a uniform half space.

The electromagnetic field at a point z in a conducting half space, due to a horizontal electric dipole buried at a depth d, can be expressed in terms of a sum of the direct field, the ideal reflected field or field of an ideal image and the rest of the field (King *et al.*[12]). This last part includes a lateral-wave field and correction terms for the reflected field to account for the fact that it may be not, actually, that of an ideal image. For instance, the radial electric field is:

$$E_R(\omega, R, \varphi, z) = -\frac{\omega\mu_0}{4\pi k^2}\cos\varphi\left[F_{R0}(R, z-d) + F_{R0}(R, z+d) + F_{R1}(R, z+d)\right]$$

where

$$F_{R0}(R, z-d) = \int_0^\infty \left(\frac{\gamma_1}{2}\left[J_0(\lambda R) - J_2(\lambda R)\right] + \frac{k_1^2}{2\gamma_1}\left[J_0(\lambda R) - J_2(\lambda R)\right]\right) e^{i\gamma_1|z-d|}\lambda d\lambda,$$

$$F_{R0}(R, z+d) = \int_0^\infty \left(\frac{\gamma_1}{2}\left[J_0(\lambda R) - J_2(\lambda R)\right] + \frac{k_1^2}{2\gamma_1}\left[J_0(\lambda R) - J_2(\lambda R)\right]\right) e^{i\gamma_1|z+d|}\lambda d\lambda,$$

$$F_{R1}(R, z+d)$$
$$= \int_0^\infty \left(\frac{\gamma_1}{2}(Q-1)\left[J_0(\lambda R) - J_2(\lambda R)\right] + \frac{k_1^2}{2\gamma_1}(P+1)\left[J_0(\lambda R) - J_2(\lambda R)\right]\right) e^{i\gamma_1|z-d|}\lambda d\lambda,$$

$$Q=\frac{k_1^2\gamma_2-k_2^2\gamma_1}{k_1^2\gamma_2+k_2^2\gamma_1},\quad P=\frac{\gamma_2-\gamma_1}{\gamma_2+\gamma_1},\quad \gamma_j=\sqrt{k_j^2-\xi^2-\eta^2}.$$

$J_j(\lambda R)$ are the Bessel functions of the first kind, medium 1 here is the Earth, medium 2 is the insulating atmosphere, k_j are the wavenumbers in media 1 and 2, and ξ, η are spatial wavenumbers of the Fourier-Bessel transform. The corresponding azimuthal magnetic field is

$$B_\varphi(\omega,R,\varphi,z)=-\frac{\mu_0}{4\pi}\cos\varphi\left[G_{\varphi 0}(R,z-d)+G_{\varphi 0}(R,z+d)+G_{\varphi 1}(R,z+d)\right]$$

where

$$G_{\varphi 0}(R,z-d)=\pm\int_0^\infty J_0(\lambda R)e^{i\gamma_1|z-d|}\lambda d\lambda\quad\begin{cases}z>d\\0\le z\le d',\end{cases}$$

$$G_{\varphi 0}(R,z+d)=\int_0^\infty J_0(\lambda R)e^{i\gamma_1(z+d)}\lambda d\lambda,$$

$$G_{\varphi 1}(R,z+d)$$
$$=\int_0^\infty\left(\frac{1}{2}(Q-1)\left[J_0(\lambda R)\pm J_2(\lambda R)\right]-\frac{1}{2_1}(P+1)\left[J_0(\lambda R)\mp J_2(\lambda R)\right]\right)e^{i\gamma_1(z+d)}\lambda d\lambda.$$

It turns out that due to the low frequencies involved in this kind of process, the lateral-wave field at the earth-air interface is insignificant and may omitted. Furthermore, and inasmuch as we are interested in the behavior of the field at intermediate-large distances from the source, we assume that the source-receiver separation is considerably greater than the depth of burial of the source, and $R \ge 5d$, $R \ge 5|z|$, so that the epicentral distance $r \sim [R^2 + (z-d)^2]^{1/2} \sim R$. At $z = 0$, (the surface of the half space), and after considerable algebra, we may express the electric field with the simple formulae:

$$E_R=\frac{\omega\mu_0\cos\varphi}{4\pi k^2}\left[\left(\frac{k}{R^2}+\frac{i}{R^3}\right)-\frac{d}{R}\left(\frac{ik}{R^2}-\frac{3}{2R^3}\right)\right]e^{ikR},\tag{6a}$$

$$E_\phi=\frac{\omega\mu_0\sin\varphi}{4\pi k^2}\left[\left(\frac{i}{R^3}-\frac{k}{R^2}\right)+i\frac{d}{R}\left(\frac{ik^2}{R}-\frac{3k}{2R^2}-\frac{5i}{8R^3}\right)\right]e^{ikR},\tag{6b}$$

$$E_z = 0 \tag{6c}$$

where k is the wavenumber in medium 1 (the earth). The corresponding expressions for the magnetic fields become

$$B_R = -\frac{\mu_0 \sin\varphi}{2\pi k}\left[\frac{ik}{R^2} - \frac{7}{2R^3} + \frac{d}{R}\left(\frac{ik^2}{R} - \frac{5k}{R^2} - \frac{12i}{R^3}\right)\right]e^{ikR}, \tag{7a}$$

$$B_\phi = -\frac{\mu_0 \cos\varphi}{2\pi k}\left[\frac{2}{R^3} + \frac{3i}{kR^4} + \frac{2d}{R}\left(\frac{k}{R^2} + \frac{3i}{R^3}\right)\right]e^{ikR}, \tag{7b}$$

$$B_z = -\frac{\mu_0 \sin\varphi}{2\pi}\left[\frac{1}{R^2} + \frac{3i}{kR^3} - \frac{3}{k^2R^4} + \frac{d}{R}\left(\frac{k}{R} + \frac{3i}{2R^2} - \frac{9}{8kR^3}\right)\right]e^{ikR}. \tag{7c}$$

4.1 Propagation and waveforms of the dipole field from a single crack

First, let us examine the dependence of the received electromagnetic field on the distance from the source (source-receiver separation). The source has a unit current moment, it is buried at d = 10000 m and its time function is assumed to be a Kronecker-δ with an infinite spectral density of unity. The results are shown in Fig. 2, for the total horizontal electric and magnetic fields propagating over distances of 50–200 km.

Figure 2a illustrates the dependence as a function of frequency (period), in an Earth medium with constant resistivity ρ = 100 Ωm. It may easily be verified that $E(R) \sim R^{-3}$ at long periods (10^4 s), changing to $E(R) \sim R^{-4}$ at shorter periods (100 s). Notably, at $T < 100$ s, the dependence appears to follow a much faster decay law, which changes from approximately R^{-5} at ranges of 50–60 km, to the extremely fast rate of R^{-10} and higher at ranges of 150–200 km. Figure 2b illustrates the corresponding dependence of the horizontal magnetic field. Differences may be observed at ranges closer to the source, where the electric field exhibits a lesser sensitivity with changing period, but, in general, the decay laws appear to be very similar. Figure 2c illustrates the dependence of the electric field as a function of resistivity at a constant period T = 500 s. An approximate R^{-3} law appears to control field decay, save for the more conductive half-space (10 Ωm), where a gradual transition from R^{-3} closer to the source, to R^{-6} at 150–200 km appears to exist. Almost identical observations can be made on the corresponding dependence of the total horizontal magnetic field (Fig. 2d).

Such behavior of the electromagnetic field may be understood from its dependence on skin depth $\delta = (1+i)/k$. Large skin depths (high resistivity-period products) imply that at distances of the order of 100–200 km, we are in near field

conditions and decay is controlled mainly by the product $\delta^{-1}R^{-2}$. Smaller skin depths amount to departure from near field conditions and decay is gradually dominated by the exponential and the R^{-2} factors. Such conditions are satisfied for combinations of large distances and high conductivities, or short periods or both. Thus, it appears that the short period (e.g. <1 s) components of the transient signal are practically impossible to propagate beyond a few tens of km, even under very favorable conditions. At large distances from the source, only the very long periods may be detectable and the received waveform will, necessarily, exhibit a very slow variation with time.

Figures 3a and 3b illustrates the electromagnetic field components from a horizontal dipole source at very low (~0°) and very high (~90°) polar angles. The fields have been obtained for the period $T = 100$ s and half-space of resistivity $\rho = 100$ Ωm. The depth of burial is 5000 m. It is apparent that the minimum horizontal electric field is observed at very low polar angles (*parallel or sub-parallel to the dipole axis*), and comprises a radial component (zero azimuthal). The maximum horizontal electric field is observed at very high polar angles (*normal or sub-normal to the dipole axis*). The same is true for the horizontal magnetic field, with the difference that at low polar angles the B-field is mainly azimuthal and at high angles it is mainly radial. Note however the very interesting behavior of the vertical magnetic field and in particular, its relationship to the horizontal. (sub)parallel to the dipole axis, the horizontal magnetic field is principally azimuthal and $B_h >> B_z$ ($B_z = 0$ at $\varphi = 0$). (Sub)normally to the dipole axis however, B_h and B_z are comparable and in fact there an area where $B_z > B_h$. The latter property is clearly illustrated in Fig. 3c, in which we have plotted B_z as a gray scale image in the entire domain where $B_z > B_h$, while the remaining (stippled) part is the area where $B_h > B_z$. The former area is roughly circular with a diameter of 100 km. As will be discussed in the following, this is an important property which may prove to be diagnostic of the source.

In a final example, Figs. 4a and 4b illustrate the received waveforms of transient fields from a single dipole source buried at $d = 10$ km and located at a distance $R = 105$ km from the receiver. The Earth has a uniform resistivity 100 Ωm. A Kronecker-δ source time function is assumed. Figure 3a is the received spectrum and Fig. 4b the half width of the waveform, computed with direct numerical integration of the spectrum. The waveform exhibits a slow decay, decreasing by approximately one order of magnitude within less than 150 s. This result should be expected from our discussion of Fig. 4: high frequencies cannot propagate far from the source, with consequence that the received spectrum becomes enriched in low frequencies and dies out slowly. We believe that this is an interesting result inasmuch as it shows how an instantaneous source may be stretched in time by many orders of magnitude, simply as an effect of its propagation over long distances through a finite conducting medium, even if it is not dispersive.

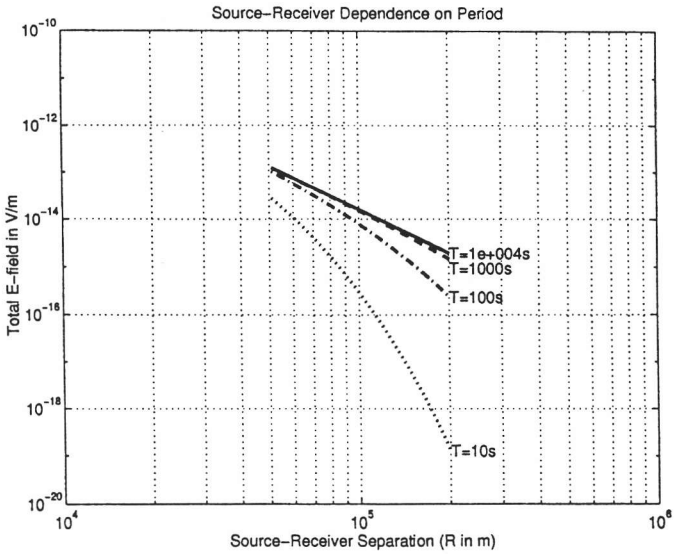

(a)

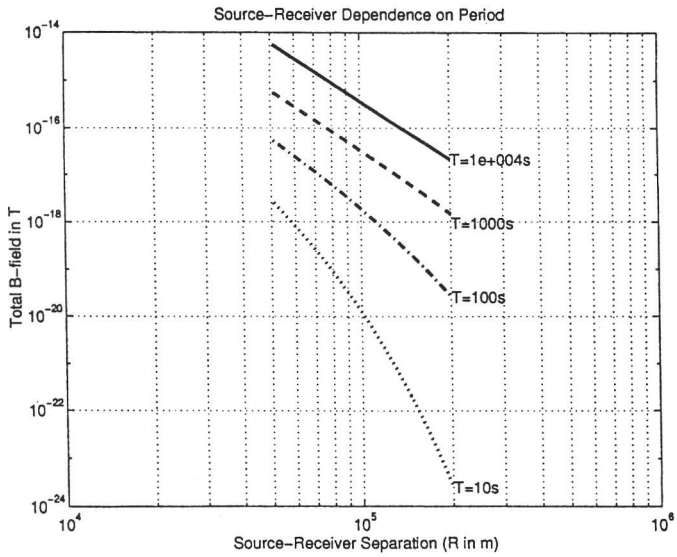

(b)

Fig. 2. (a) Attenuation of the horizontal electric field from a unit dipole crack as a function of source-receiver separation (R) for different periods. (b) Attenuation of the horizontal magnetic field from a unit dipole crack as a function of source-receiver separation (R) for different periods. (c) Attenuation of the horizontal electric field from a unit dipole crack as a function of source-receiver separation (R) for different resistivities of the earth medium. (d) Attenuation of the horizontal magnetic field from a unit dipole crack as a function of source-receiver separation (R) for different resistivities of the earth medium.

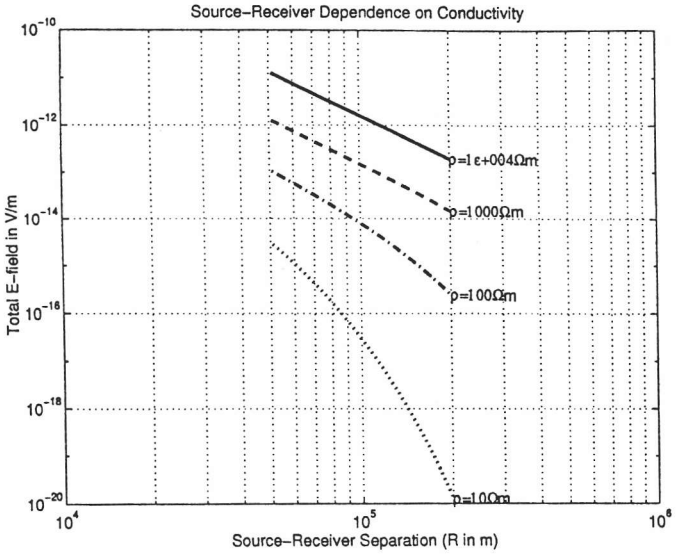

(c)

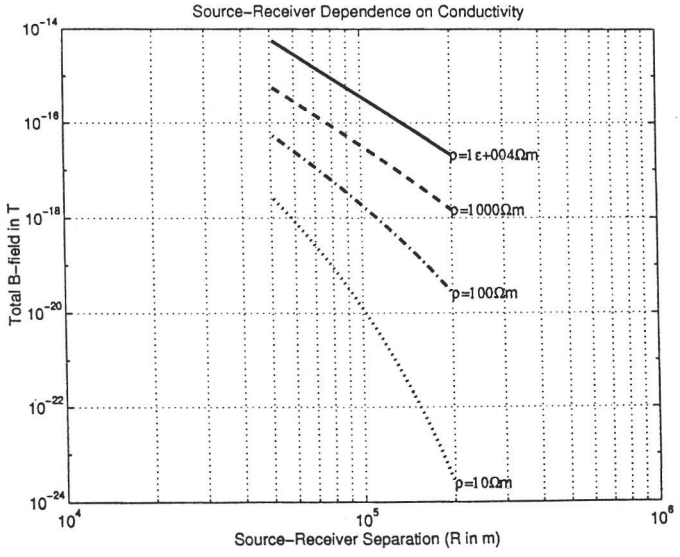

(d)

Fig. 2. (continued).

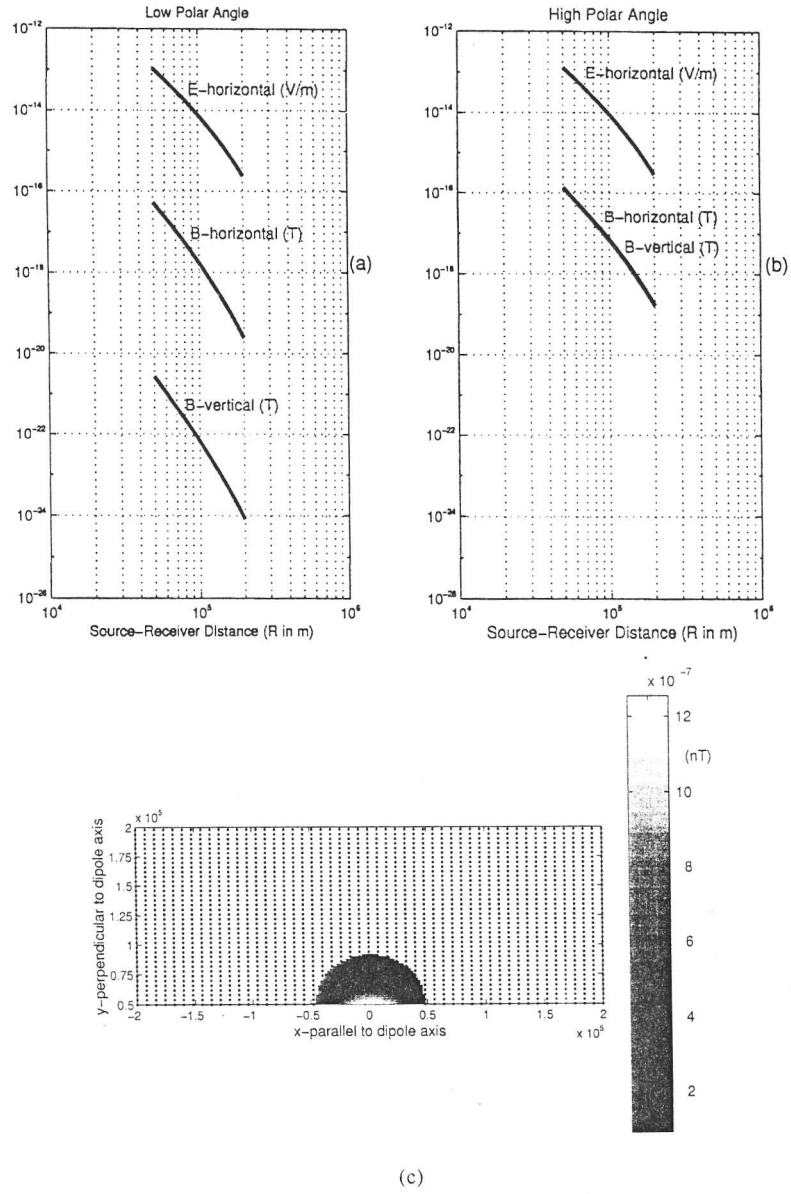

(c)

Fig. 3. Attenuation of the electric and magnetic fields from a unit dipole crack as a function of source-receiver separation (R) at very low polar angles (a) and very high polar angles (b). The dipole is positive-x oriented and buried at $d = 5000$ m, the period is 100 s and the earth medium comprises a half-space with resistivity $\rho = 100$ Ωm. (c) Map showing B_z as a gray scale image in the entire domain where the vertical magnetic field is greater than the horizontal ($tB_z > B_h$); the remaining (stippled) part is the area where $B_h > B_z$. The dipole is configured as per (b).

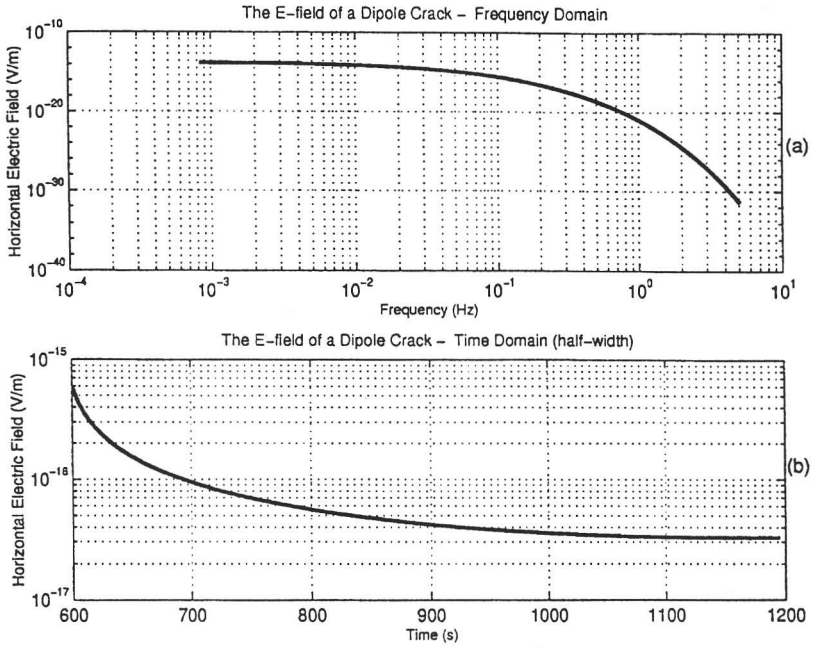

Fig. 4. (a) The spectrum of the electric field of a dipole source, at a distance R = 105 km from the source. A Kronecker-δ source time function is assumed. The spectrum is normalized so that E_h (100 s) = 1.12×10^{-14} V/m (see the text for an explanation). (b) The waveform of the electric field with the spectrum of (a), received at a distance R = 105 km from the source.

4.2 Propagation and waveforms of the field from multiple cracks (an excited cell)

In Subsection 4.1, we have presented the properties of the field emitted by a single crack. If, however, the cracks in a cell within the seismogenic volume are excited coherently, the resulting field will be the superposition of the fields from each individual crack. In a strained crustal volume, the only cracks that may propagate are (sub)parallel to the intermediate stress axis (σ_2) and (sub)normal to the plane $\sigma_1\sigma_3$ defined by the maximum compressive and minimum tensional stresses respectively (for a comprehensive account see Scholz[13] and references therein). Therefore, the long dipole axis should be aligned with the direction of propagation of the crack and therefore, should be (sub)parallel to the fault. Thus, the maximum E_R (maximum B_Φ) will be (sub)parallel to the fault, and the maximum E_Φ (maximum B_R) will be normal to the fault. In the following we will consider the case of $\varphi = 90°$ (fields normal to the fault).

Consider a 1 Am dipole source buried at d = 5000 m in a half space with ρ = 100 Ωm. If T = 100 s, then at R = 100 km the total horizontal electric and magnetic fields are respectively $E_h = 8.7 \times 10^{-15}$ V/m and $B_h = 6.28 \times 10^{-18}$ T. For an estimate of the actual current through an individual excited dipole crack, we

have to rely on laboratory measurements. Warwick *et al.*[14], has found that $i_c \sim 10^{-3}$ A. Molchanov and Hayakawa[15] indicate that typical lengths of microcracks and microfractures (clusters of dislocations) are of the order 10^{-4}–10^{-1} m). We assume a mean length $l_c = 10^{-3}$ m. If a relatively rapid strain change occurs, then some elementary crustal volume will acquire new cracks. The maximum number of cracks containable in a unit volume is controlled by their size. Gershenzon *et al.*[16] provide the relationship

$$N_{\max} = (3 \cdot \tau \cdot \upsilon)^{-3}$$

where $N_{\max}$ is the maximum crack density, τ is the time and υ is the velocity of crack opening. Assuming a constant velocity for crack opening $\upsilon = 10^3$ m/s, (comparable to seismic velocities), we find $\tau = 10^{-6}$ s and $N_{\max} = 3.7 \times 10^7$ m^{-3}. If $N_{\max}$ cracks are coherently excited in a volume $V \sim 10^7$ m^3 then at a distance of 100 km from the source the received horizontal electric and magnetic fields will be

$$E \sim N_{\max} \cdot V \cdot i_c \cdot l_c \cdot E_h \sim 3.2 \times 10^{-6} \text{ V/m} = 3.2 \text{ mV/km},$$

$$B \sim N_{\max} \cdot V \cdot i_c \cdot l_c \cdot B_h \sim 2.3 \times 10^{-9} \text{ T} = 2.3 \text{ nT}.$$

This is a correct order of magnitude of electrical earthquake precursors, but it also comprises an upper limit. In order to obtain this amplitude (at $T = 100$ s), we require the maximum coherent excitation of a cell with dimensions $215 \times 215 \times 215$ m.

A free parameter in this consideration however, is our estimate of N. For instance, if $N \sim 10^5$ and all other parameters are kept constant, the necessary dimensions of the excited cell (i.e. the effective volume V) should rise to 1 km^3. We do not know what a realistic N may be and order of magnitude variations should be expected within the earthquake preparation zone. For instance, domains of increased fracturation (the fault zone), or domains of increased loading (asperities and barriers) may be expected to have higher N values. According to Gershenzon *et al.*[16] inside the earthquake preparation zone "*strain is distributed in a mosaic manner, with regions of large strain ... alternating with those where* $\varepsilon = 0$. *The distribution of strain over depth is also complex ...*". Thus, it should be expected that $N < N_{\max}$ and changing with time; it may reach the maximum value only at the time of failure[16]. Accordingly, the effective volume required to produce a 3 mV/km/2 nT amplitude at $T = 100$ s will be larger, or the signal weaker. It follows that for the MCD model to work, we require the collective or individual excitation of distributed cells with dimensions of the order of 1 km^3 and strain rates of the order of 10^{-12}–10^{-11} s^{-1}.

Now, consider that a M5.5 earthquake has typical fault dimensions of 10 km $\times$ 7 km and affects a crustal volume of 4.6×10^{11} m^3, i.e. the average width of the seismogenic zone is 6.5 km. It is not expected that the entire seismogenic zone

will, or can be excited. We expect that conditions sufficient to trigger the generation of current are limited in a sub-volume in the neighborhood of the fault. If this sub-volume is only $10 \times 7 \times 1$ km, (7×10^{10} m^3), it still is 10–10^2 times larger than the elementary cell sufficient to provide a 3 mV/km/2 nT signal. In the case of a M6.5 event, these dimensions respectively become 30×12 km, the volume is 1.4×10^{13} m^3 and the width 38 km. Again, if conditions sufficient for excitation exist only in a volume $30 \times 12 \times 5$ km around the fault, this still is 10^3–10^6 times larger that that sufficient to give a 3 mV/km/2 nT variation. Therefore, it is conceivable that a sufficient number of cells above the effective volume threshold may appear in the seismogenic zone. If small cells are excited or small earthquakes are concerned, signals may not be observed even at close ranges, not because they are not generated, but because they're very weak to detect.

An important question is that of the temporal behavior of cell excitation and the duration of the source. We cannot provide some affirmative answer to this problem. Thus, and depending on conditions particular to the seismogenic zone in question, the entire zone may emit uniformly, or discretely in time (each cell on its own, when and if it is excited). The absolute lower limit for the duration of the source is τ (all the cracks in a cell emit simultaneously). In the general case, the duration will be a function of the pace at which strain builds up and propagates in the seismogenic zone. Consider however, that when strain increases older cracks propagate and new cracks appear. Thus N increases and the effective excitation volume decreases. New, smaller cells may pass the excitation threshold and jump into action. This process will continue and may accelerate until the strain rate drops below the required threshold, upon which time it decelerates and stops. The duration of this process is unknown, but may, conceivably, require several seconds or even minutes. Note also that the duration of experimentally observed pre-seismic signals indicates that the most favorable case is the one of high deformation over small volumes within time constants of several minutes to a few hours—a very plausible situation when the crustal material is undergoing rapid non-linear changes near the failure threshold.

To investigate this point, we examine waveforms of transient electric fields from an excited cell buried at $d = 10$ km and located at a distance $R = 105$ km from the receiver. The Earth has a uniform resistivity of 100 Ωm. In order to study the effects of source spectrum on the propagation of the EM field, we consider two Dirac-δ types of source time functions: a faster with duration of 60 s, which is richer in higher frequencies (continuous line) and a slower with duration 400 s, richer in lower frequencies (dashed line). Figure 5a shows the received spectrum, (the product of the spectrum of a unit amplitude Kronecker-δ type source, times the modulus of the spectrum of the time function, normalized to 4×10^{-6} V/m at $T = 1000$ s). Figure 5b is the corresponding time domain variation—shown in a relative time scale—computed from the spectrum with direct numerical integration (assuming the practical and realistic case that all frequencies arrive simultaneously from the source). Observe that the waveforms look like depressed and

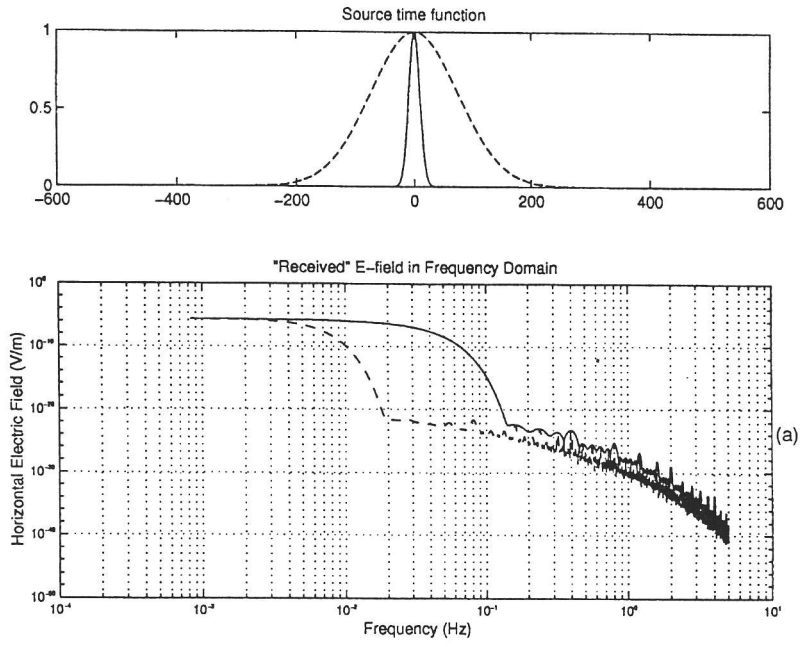

(a)

Fig. 5. (a) The time function of a "fast" (continuous line) and a "slow" (dashed line) excited crustal cell and the corresponding spectra, of the horizontal electric field received at a distance $R = 105$ km from the source. The spectra have been normalized so that $E_h\,(T = 1000\text{ s}) = 4 \times 10^{-6}$ V/m. (b) The time function of a "fast" (continuous line) and a "slow" (dashed line) excited crustal cell and the corresponding waveform of the horizontal electric field. (c) The time function (continuous line) and the "received" waveform (dashed line), of a composite source with a sharp onset and a slower decay.

stretched replicas of the source time functions. When compared to each other, the faster source (continuous line) has a sharper onset, shorter duration and considerably faster decay than the slower source. These are effects of the source spectrum: the slower it is, the richer in low frequencies, which experience lower attenuation and dominate the received spectrum stretching the shape and the duration of the waveform. In order to further explore this point, we present Fig. 5c, illustrating the full "received" waveform (dashed line) of a composite source function comprising a sharp onset and a slower decay (continuous line). Both the time function and the received waveform have been normalized to unity. Observe that (within the accuracy of the computations), the transient field has been stretched and smoothed as a consequence of high frequency attenuation, although some basic features of its original structure are still recognizable (its rise time is steeper than its decay time). The duration of the waveform is considerably longer than the

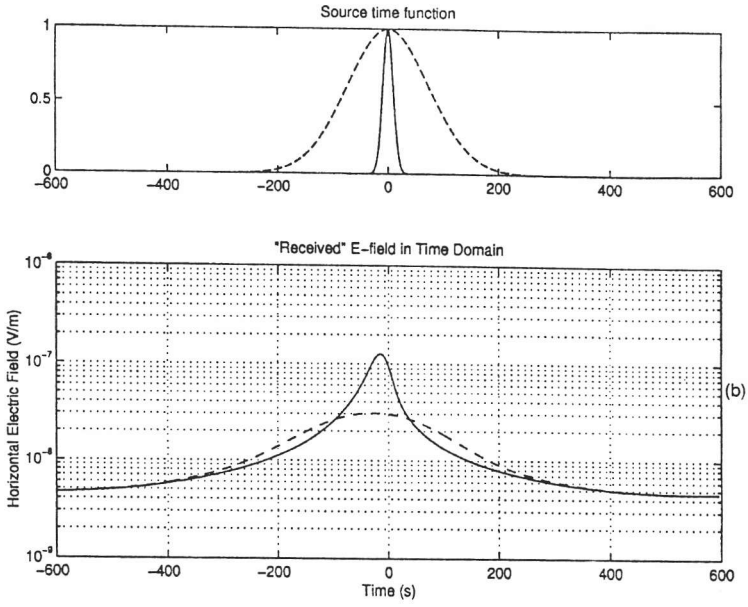

(b)

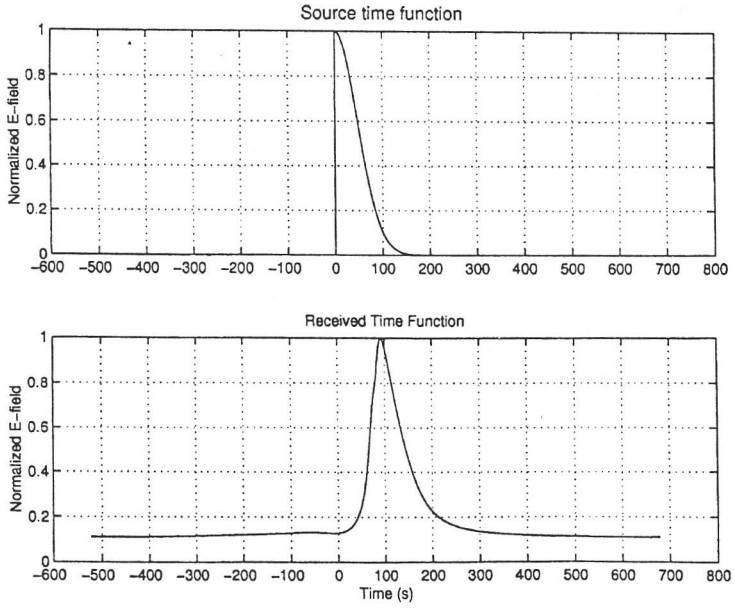

(c)

Fig. 5. (continued).

duration of the source. In a concluding remark, we note that the simulated waveforms of Figs. 4b and 5c, 5 exhibit several features reminiscent of some classes of bay-like variations, claimed to have been observed prior to earthquakes by several authors[6),17)–21)].

5. Concluding Remarks

In the foregoing we have attempted to describe the pre-seismic transient current generation mechanism in terms of the Moving Charged Dislocation (MCD) model. We expand the hypothesis that the source of a pre-seismic (or co-seismic) transient electric variation may be the generation of an electric current in the earthquake focus due to the non-linear evolution of deformation during the preparation stage of an earthquake. Towards this effect, we have estimated the appropriate stress sensitivity coefficient, $E/(d\sigma/dt)$, necessary to initiate excitation of a rock volume. The resulting values are comparable with that calculated using the experimental data for different types of rocks. We provide a model which associates current density and the electric field with the rate of deformation ($\dot{\varepsilon}$) and we also derive order of magnitude estimates of the strain rates necessary to initiate current generation. These estimates are high with respect to long-term geological strain rates and well above the tidal level (as they should be expected, otherwise the crust would be in a state of continuous excitation). Moreover, when "normalized" by the fact that our calculations have been made on the basis of some drastic assumptions (homogeneous, linear, isotropic material), as well as laboratory data obtained under controlled conditions, the resulting estimates are not at all implausible. In fact, they are comparable to the observed strain rates of a large Japanese event. We believe that this result is significant in assessing the physical conditions appropriate for the generation of a pre-seismic signal and hence the validity of the MCD model.

We expand our exploration of the appropriate physical conditions of the earthquake preparation zone, by evaluating the size of the earthquake source volume capable of yielding a MCD signal observable at long distances from the source. We find that providing that the MCD model is capable of generating sufficient current in real Earth conditions, the observation of electric fields at intermediate-long distances is feasible for intermediate and large size events. Furthermore, we construct models of such waveforms which turn out to possess bay-like shapes, resembling some classes of signals observed by several independent investigators prior to earthquakes.

The MCD model considered herein also predicts the generation of three component magnetic fields. The predicted amplitude of the magnetic field is certainly observable with modern instrumentation (sensitive fluxgates and induction coils). In fact, it is 1–2 orders of magnitude above the Schumann background which is routinely used in MT soundings[22)]. However it is also at least one order of magnitude lower than a typical geomagnetic disturbance of similar duration,

so that considerable caution needs to be exercised for its observation and evaluation. At any rate, the MCD magnetic field should exhibit considerable azimuthal dependence, which is also used as diagnostic of the source quality and properties.

The model presented herein is by all means preliminary and certainly not proven. Although many of its components are demonstrable or physically arguable, there still exist several free parameters (the effective excitation volume at the earthquake zone to mention one), which require considerable effort before they can be tuned: the successful conclusion of such an undertaking is by no means certain. Nevertheless, we believe that we have presented enough evidence to demonstrate that the MCD process due to strain rate changes is geophysically plausible and a solid candidate generator of electrical earthquake precursors.

REFERENCES

(1) Whitworth, R. W., 1975, *Adv. Phys.*, **24**, 203–304.
(2) Hadjicontis, V. and Mavromatou, C., 1994, *Geophys. Res. Lett.*, **21**, 1687–1690.
(3) Varotsos, P., Alexopoulos, K. and Lazaridou, M., 1993, *Tectonophysics*, **224**, 1–37.
(4) Slifkin, L., 1993, *Tectonophysics*, **224**, 149–152.
(5) Vallianatos, F., 1996. Electric current generation in rocks under pressure, *Proceedings, XII Congress in Solid State Physics*, Heraklion, Crete, 15–18 September 1996 (in press).
(6) Nomikos, K. and Vallianatos, F., 1997, *Tectonophysics*, **269**, 171.
(7) Teisseyre, R., 1987, *Phys. Earth Planet. Inter.*, **49**, 24–29.
(8) Ernst, T., Jankowski, J., Rozluski, C. and Teisseyre, R., 1993, *Tectonophysics*, **224**, 141–148.
(9) Myachkin, V. I., Kostrof, B. V., Sobolev, G. A. and Shamina O. G., 1986, in *Physics of the Earthquake Focus*, ed. by M. A. Sadovskii, Balkema, Rotterdam, pp. 1–26.
(10) Stuart, W. D., 1988, *Pure Appl. Geophys.*, **126**, 619–641.
(11) Wakita, H., 1988, *Pure Appl. Geophys.*, **126**, 267–278.
(12) King, R. W. P., Owens, M. and Wu. T. S., 1992, *Lateral Electromagnetic Waves*, Springer Verlag.
(13) Scholz, C. H., 1990, *The Mechanics of Earthquakes and Faulting*, Cambridge University Press.
(14) Warwick, J. W., Stoker, C. and Meyer, T. R., 1982, *J. Geophys. Res.*, **87**, 2851–2859.
(15) Molchanov, O. V. and Hayakawa, M., 1995, *Geophys. Res. Lett.*, **22**, 3091–3094.
(16) Gershenzon, N. I., Gokhberg, M. B., Kakarin, A. V., Petviashvili, N. V. and Rykunov, A. L., 1989, *Phys. Earth Planet. Inter.*, **57**, 129–138.
(17) Sobolev, G. A., 1975, *Pure Appl. Geophys.*, **113**, 229.
(18) Sobolev, G. A., Bogaevskii, V. N., Lementueva, R. A., Mugunov, N. I. and Khromov, A. A., 1986, in *Physics of the Earthquake Focus*, ed. by M. A. Sadovskii, Balkema, Rotterdam, pp. 196–234.
(19) Varotsos, P. and Alexopoulos, K., 1984a, *Tectonophysics*, **110**, 73–98.
(20) Varotsos, P. and Alexopoulos, K., 1984b, *Tectonophysics*, **110**, 99–125.
(21) Varotsos, P. and Alexopoulos, K., 1987, *Tectonophysics*, **136**, 335–339.
(22) Tzanis, A. and Beamish, D., 1987, *J. Geophys.*, **61**, 97–109.